Global analysis of a minimally extended scotogenic model

Huchan Lee

Seoul National University of Science and Technology (SeoulTech)

arXiv: 2606.26752

In collaboration with Prof. Sin Kyu Kang

August 19, 2026

Table of Contents

1. Introduction

The Standard Model has successfully described a wide range of phenomena with remarkable precision.

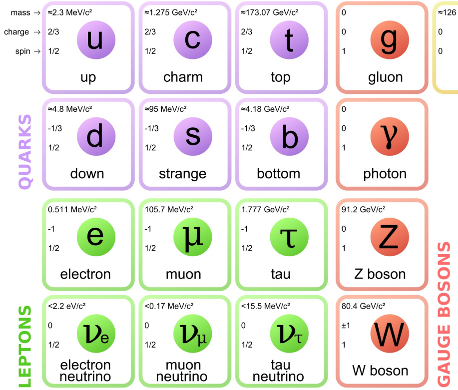

Limitations of the SM:

- Non-zero neutrino masses
- Dark Matter (DM) and Dark Energy (DE)
- Instability of the SM vacuum at high energy
- Baryon asymmetry
- flavor puzzle: hierarchy in fermion masses and mixing pattern

1. Introduction

The main motivations for this work are as follows:

1. To construct a minimal extension of the SM that accounts for non-zero neutrino masses, provide a viable dark matter candidate, and stabilizes the electroweak (EW) vacuum by investigating
   - bounded-from-below conditions
   - Vaccum stability
   - Renormalization-Group-deriven perturbative bounds
2. To determine whether the normal or inverted mass hierarchy is further constrained within this framework.
3. To identify which flavor observables will be accessible in near-future experiments.
   - Muon anomalous magnetic moment and radiative $\ell_\alpha \to \ell_\beta \gamma$ decays
   - $\ell_\alpha \to 3\ell_\beta$ decays and $\mu \to e$ conversion rate.
   - EW precision observable: oblique parameters
   - EW precision observable: leptonic decays of Z/H

Table of Contents

2. Model

The minimally extended scotogenic model is given in Table 1:

Field	Q_i	u_i^c	d_i^c	L_i	e_i^c	N_i^c	H	η	S
$SU(3)_C$	$\mathbf{3}$	$\bar{\mathbf{3}}$	$\bar{\mathbf{3}}$	$\mathbf{1}$	$\mathbf{1}$	$\mathbf{1}$	$\mathbf{1}$	$\mathbf{1}$	$\mathbf{1}$
$SU(2)_L$	$\mathbf{2}$	$\mathbf{1}$	$\mathbf{1}$	$\mathbf{2}$	$\mathbf{1}$	$\mathbf{1}$	$\mathbf{2}$	$\mathbf{2}$	$\mathbf{1}$
$U(1)_Y$	$\frac{1}{6}$	$-\frac{2}{3}$	$\frac{1}{3}$	$-\frac{1}{2}$	1	0	$\frac{1}{2}$	$\frac{1}{2}$	0
Z_2	1	1	1	1	1	-1	1	-1	1
$U(1)_X$	0	0	0	-1	1	1	0	0	-2

Table 1: Particle content of the minimally extended scotogenic model.

The Lagrangian with the field assignment is:

$$\mathcal{L}_{\mathrm{ren}} = y_u Q_i \widetilde{H} u_i^c - y_d Q_i H d_i^c - y_e L_i H e_i^c + g_X L_i \eta N_i^c + \frac{g_R}{2} S N_i^c N_i^c + \mathrm{h.\,c.}\,. \tag{1}$$

And the scalar potential is:

$$\begin{aligned} V_{\mathrm{ren}} = &-\mu_H^2 H^\dagger H + \mu_\eta^2 \eta^\dagger \eta - \mu_S^2 S^* S - \frac{1}{2}\mu_{\mathrm{sb}}^2 (S^2 + S^{*,2}) \\ &+ \frac{1}{4}\lambda_1 (H^\dagger H)^2 + \frac{1}{4}\lambda_2 (\eta^\dagger \eta)^2 + \lambda_3 (H^\dagger H)(\eta^\dagger \eta) + \lambda_4 (H^\dagger \eta)(\eta^\dagger H) \\ &+ \frac{1}{4}\lambda_5 \left[(\eta^\dagger H)^2 + h.c.\right] + \frac{1}{4}\lambda_6 (S^* S)^2 + \lambda_7 (H^\dagger H)(S^* S) + \lambda_8 (\eta^\dagger \eta)(S^* S) \end{aligned} \tag{2}$$

2. Model

After SSB, the scalar fields are:

$$H=\begin{pmatrix} G^+ \\ \frac{1}{\sqrt{2}}\left(v+\phi_{H0}+i\sigma_{H0}\right) \end{pmatrix}, \quad \eta=\begin{pmatrix} \eta^+ \\ \frac{1}{\sqrt{2}}\left(\eta_R+i\eta_I\right) \end{pmatrix}, \quad S=\frac{1}{\sqrt{2}}\left(v_S+\phi_S+i\sigma_S\right), \tag{3}$$

And the CP-even mass matrix reads:

$$M^2_{\text{CP-even}}=\begin{pmatrix} \frac{1}{4}\left(-4\mu_H^2+3\lambda_1 v^2+2\lambda_7 v_S^2\right) & \lambda_7 v v_S \\ \lambda_7 v v_S & \frac{1}{4}\left(-4\left(\mu_S^2+\mu_{\text{sb}}^2\right)+2\lambda_7 v^2+3\lambda_6 v_S^2\right) \end{pmatrix} \tag{4}$$

The diagonalization for the CP-even mass matrix is:

$$U^H M^2_{\text{CP-even}} U^{H,T}=M^{\text{diag},2}_{\text{CP-even}}, \left(h_1 h_2\right)^T=U_H^T\left(\phi_{H0},\phi_S\right)^T. \tag{5}$$

For the RH neutrino mass matrix diagonalization is:

$$M_\chi^{\text{flavor}}=\frac{1}{\sqrt{2}}g_R^{ij}v_S,\ \ i,j=1,2,3\ ,U^{\chi,*}M_\chi^{\text{flavor}}U^{\chi,\dagger}=M_\chi^{\text{diag}}. \tag{6}$$

2. Model

2.1 Neutrino mass generation

The diagram for neutrino mass generation is (Z_2 symmetry forbids tree-level ν mass generation):

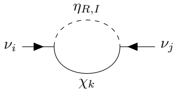

Figure 1: Neutrino mass generation at one-loop level

The flavor neutrino mass matrix at one-loop level is:

$$\mathcal{M}_\nu = g_X^T M_L g_X$$

where M_L is a complex symmetric 3×3 matrix which encodes loop functions and scalalr and fermion mixing matrices.

$$M_L^{i,j} = \frac{1}{2} \sum_{k=1}^{3} \left(b_{\text{loop}} \left(\eta_R, k \right) - b_{\text{loop}} \left(\eta_I, k \right) \right) \left(U_{(k,i)}^{\chi,*} \right) \left(U_{(k,j)}^{\chi,*} \right) \tag{7}$$

where the loop function b_{loop} is defined as $b_{\text{loop}} \left(\phi, k \right) = \dfrac{1}{16\pi^2} \dfrac{M_\chi^k}{M_\phi^2 - M_\chi^{k,2}} \left(M_\phi^2 \ln \dfrac{M_\phi^2}{M_\chi^{k,2}} \right)$. The 3×3 Yukawa coupling matrix g_X can be written using the Casas-Ibarra parameterization:

$$g_X = U_L^\dagger D_L^{-1/2} U_R D_\nu^{1/2} U_{\text{PMNS}}^T, \quad \left(D_L = U_L^T M_L U_L \right)$$

	Normal hierarchy		Inverted hierarchy	
	1σ range	3σ range	1σ range	3σ range
$\sin^2_{\theta_{12}}$	$0.3088^{+0.0067}_{-0.0066}$	$0.2893 \to 0.3295$	$0.3088^{+0.0067}_{-0.0066}$	$0.2893 \to 0.3295$
$\theta_{12}/^\circ$	$33.76^{+0.42}_{-0.41}$	$32.54 \to 35.03$	$33.76^{+0.42}_{-0.41}$	$32.54 \to 35.03$
$\sin^2_{\theta_{23}}$	$0.470^{+0.017}_{-0.014}$	$0.432 \to 0.587$	$0.555^{+0.013}_{-0.016}$	$0.437 \to 0.590$
$\theta_{23}/^\circ$	$43.27^{+1.00}_{-0.82}$	$41.11 \to 50.02$	$48.15^{+0.75}_{-0.92}$	$41.40 \to 50.21$
$\sin^2_{\theta_{13}}$	$0.02249^{+0.00057}_{-0.00057}$	$0.02070 \to 0.02420$	$0.02261^{+0.00056}_{-0.00056}$	$0.02091 \to 0.02433$
$\theta_{13}/^\circ$	$8.62^{+0.11}_{-0.11}$	$8.27 \to 8.95$	$8.65^{+0.11}_{-0.11}$	$8.31 \to 8.97$
$\delta_{CP}/^\circ$	207^{+23}_{-20}	$114 \to 405$	283^{+24}_{-28}	$202 \to 347$
$\frac{\Delta m^2_{21}}{10^{-5}\,\mathrm{eV}^2}$	$7.537^{+0.094}_{-0.100}$	$7.236 \to 7.823$	$7.537^{+0.094}_{-0.100}$	$7.236 \to 7.822$
$\frac{\Delta m^2_{3l}}{10^{-3}\,\mathrm{eV}^2}$	$2.521^{+0.026}_{-0.018}$	$2.454 \to 2.592$	$-2.500^{+0.024}_{-0.023}$	$-2.569 \to -2.430$

Table 2: Recent neutrino experimental data given by NuFit 6.1 [1]

	Normal hierarchy		Inverted hierarchy
m_{ν_3}	$\sqrt{m^2_{\nu_2} + \Delta m^2_{32}}$	m_{ν_2}	$\sqrt{m^2_{\nu_1} + \Delta m^2_{21}}$
m_{ν_2}	$\sqrt{m^2_{\nu_1} + \Delta m^2_{21}}$	m_{ν_1}	$\sqrt{m^2_{\nu_3} + \lvert\Delta m^2_{31}\rvert}$
m_{ν_1}	$[10^{-19}, 10^{-10}]$	m_{ν_3}	$[10^{-19}, 10^{-12}]$

Table 3: Neutrino mass hierarchy implemented in this work. All masses are in unit of GeV.

In this model, there are three DM candidates:

$$\eta_{R,I}\,, \chi_1 \tag{8}$$

The experimental value of the relic density at 68% confidence level (C.L.) is:

$$\Omega_{\mathrm{CDM}} h^2 = 0.1200 \pm 0.0012$$

$$\Omega_{\mathrm{CDM}} h^2 = 0.1200 \pm 0.0120$$

What we will fit in this work is

- Relic density
- Proton spin-independent cross section

Table of Contents

3. Scalar potential constraints

3.1 Bounded-from-below conditions and vacuum stability

In order to derive the BFB conditions, it is enough to consider the quartic terms in the scalar potential:

$$\begin{aligned} V_4 = {} & \frac{1}{4}\lambda_1 (H^\dagger H)^2 + \frac{1}{4}\lambda_2 (\eta^\dagger \eta)^2 + \lambda_3 (H^\dagger H)(\eta^\dagger \eta) + \lambda_4 (H^\dagger \eta)(\eta^\dagger H) \\ & + \frac{1}{4}\lambda_5 \left[\eta^{\dagger,2} H^2 + h.c.\right] + \frac{1}{4}\lambda_6 (S^* S)^2 + \lambda_7 (H^\dagger H)(S^* S) + \lambda_8 (\eta^\dagger \eta)(S^* S), \end{aligned} \tag{9}$$

The derived BFB conditions are:

$$\begin{aligned} \lambda_{1,2,6} &> 0 \\ \lambda_8 + \frac{1}{2}\sqrt{\lambda_2 \lambda_6} &> 0 \\ \lambda_7 + \frac{1}{2}\sqrt{\lambda_1 \lambda_6} &> 0 \\ \lambda_3 + \frac{1}{2}\sqrt{\lambda_1 \lambda_2} &> 0 \\ \lambda_3 + \lambda_4 + \frac{1}{2}\sqrt{\lambda_1 \lambda_2} &> \frac{1}{2}|\lambda_5| \\ \lambda_a \frac{\sqrt{\lambda_1 \lambda_2}}{\lambda_6} + \lambda_4 &> \frac{1}{2}|\lambda_5| \end{aligned}$$

where λ_a is

$$\frac{3}{4}\lambda_6 + \frac{\lambda_3 \lambda_6}{\sqrt{\lambda_1 \lambda_2}} + \lambda_7 \sqrt{\frac{\lambda_6}{\lambda_1}} + \lambda_8 \sqrt{\frac{\lambda_6}{\lambda_2}}.$$

The SM scalar potential is known to lie near the border between stability and metastability, primarily due to

- the experimental uncertainties in the top quark mass
- the strong coupling constant [2, 3]

Ref [3] quantified this proximity using two top quark mass determinations:

- the pole mass $M_t^\sigma = (172.4 \pm 0.7)\,\mathrm{GeV}$ - It requires a 1.9σ downward shift from its central value to achieve stability
- the MC mass $M_t^{\mathrm{MC}} = (172.57 \pm 0.29)\,\mathrm{GeV}$ - a 5.1σ shift.

Furthermore, the strong coupling constant $\alpha_S^{(5)}(M_Z)$ requires a 3.7σ upward shift from the PDG world average to stabilize the potential.

3. Scalar potential constraints

3.2 Renormalization-Group-driven perturbative bounds

It is important to determine up to which energy scale a given theory remains perturbatively valid.

1. Perturbativity must be maintained across the entire energy range over which the theory is considered to be valid, not only at the scale where the initial conditions are imposed.
2. In general, RG-improved perturbativity bounds place stronger constraints on the parameter space than the conventional bounds $g_i, y_i \leq \sqrt{4\pi}$ and $\lambda_i \leq 4\pi$.

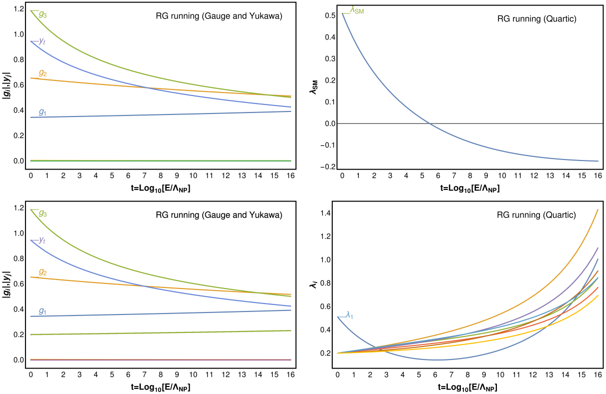

Figure 2: RG evolution of the SM (upper panels) and the scotogenic model under study (lower panels).

Table of Contents

The muon $g-2$ state has been updated as follows:

$$\Delta a_\mu = a_\mu^{\rm exp} - a_\mu^{\rm SM} = (2.49 \pm 0.48) \times 10^{-9}, \quad (5.1\sigma)$$

$$\Delta a_\mu = a_\mu^{\rm exp} - a_\mu^{\rm SM} = (0.38 \pm 0.63) \times 10^{-9}, \quad (0.6\sigma),$$

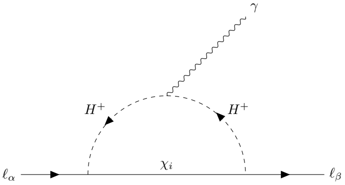

Figure 3: Diagram contributing to the muon anomalous magnetic moment and the charged lepton flavor violation (CLFV) $\ell_\alpha \to \ell_\beta\gamma$ decays.

$$\Delta a_\mu = -4\frac{m_\mu}{e}\,\mathrm{Re}\left(c_R^{\mu\mu}\right),$$

$$\mathrm{BR}\left(\ell_\alpha \to \ell_\beta\gamma\right) = \frac{m_{\ell_\alpha}^3}{4\pi\Gamma_{\ell_\alpha}}\left[|c_R^{\alpha\beta}|^2 + |c_R^{\beta\alpha}|^2\right].$$

The muon $g-2$ and the radiative decay can be expressed in terms of the coefficient of the dipole operator $c_R^{\alpha\beta}\overline{\ell}_\beta\sigma_{\mu\nu}P_R\ell_\alpha F^{\mu\nu} + \mathrm{h.c.}$ from an effective field theory (EFT) perspective.

$$c_R^{\alpha\beta} = \frac{e}{16\pi^2}\left[\Gamma_L^{\alpha *}\Gamma_R^{\beta}\frac{M_\Psi}{M_\Phi^2}\left(f(x) + Qg(x)\right) + \frac{m_{\ell_\beta}\Gamma_L^{\alpha *}\Gamma_L^{\beta} + m_{\ell_\alpha}\Gamma_R^{\alpha *}\Gamma_R^{\beta}}{M_\Phi^2}\left(\widetilde{f}(x) + Q\widetilde{g}(x)\right)\right]$$

$$f(x) = \frac{x^2 - 1 - 2x\ln(x)}{4(x-1)^3},$$

$$g(x) = \frac{x - 1 - \ln(x)}{2(x-1)^2},$$

$$\widetilde{f}(x) = \frac{2x^3 + 3x^2 - 6x + 1 - 6x^2\ln(x)}{24(x-1)^4},$$

$$\widetilde{g}(x) = \frac{x^2 - 1 - 2x\ln(x)}{8(x-1)^3}.$$

4. Flavor and electroweak observables

4.2 EW precision observable: oblique parameters

The oblique parameters quantify radiative NP corrections in BSM frameworks. They are parameterized by six quantities: S, T, U, V, W and X:

$$\frac{\alpha}{4s_w^2c_w^2}S = \frac{A_{ZZ}\left(m_Z^2\right)-A_{ZZ}\left(0\right)}{m_Z^2} - \left.\frac{\partial A_{\gamma\gamma}\left(p^2\right)}{\partial p^2}\right|_{p^2=0} - \frac{c_w^2-s_w^2}{c_w s_w}\left.\frac{\partial A_{\gamma Z}\left(p^2\right)}{\partial p^2}\right|_{p^2=0}$$

$$\alpha T = \frac{A_{WW}\left(0\right)}{m_W^2} - \frac{A_{ZZ}\left(0\right)}{m_Z^2}$$

$$\frac{\alpha}{4s_W^2}U = \frac{A_{WW}\left(m_W^2\right)-A_{WW}\left(0\right)}{m_W^2} - c_W^2\frac{A_{ZZ}\left(m_Z^2\right)-A_{ZZ}\left(0\right)}{m_Z^2} - s_W^2\left.\frac{\partial A_{\gamma\gamma}\left(p^2\right)}{\partial p^2}\right|_{p^2=0} - 2c_w s_w\left.\frac{\partial A_{\gamma Z}\left(p^2\right)}{\partial p^2}\right|_{p^2=0}$$

$$\alpha V = \left.\frac{\partial A_{ZZ}\left(p^2\right)}{\partial p^2}\right|_{p^2=m_Z^2} - \frac{A_{ZZ}\left(m_Z^2\right)-A_{ZZ}\left(0\right)}{m_Z^2}$$

$$\alpha W = \left.\frac{\partial A_{WW}\left(p^2\right)}{\partial p^2}\right|_{p^2=m_W^2} - \frac{A_{WW}\left(m_W^2\right)-A_{WW}\left(0\right)}{m_W^2}$$

$$\frac{\alpha}{s_w c_w}X = \left.\frac{\partial A_{\gamma Z}\left(p^2\right)}{\partial p^2}\right|_{p^2=0} - \frac{A_{\gamma Z}\left(m_Z^2\right)-A_{\gamma Z}\left(0\right)}{m_Z^2}$$

$A_{VV'}$ represents the transverse components of the $V-V'$ vacuum polarization tensors:

$$\Pi^{\mu\nu}_{VV'}\left(p\right) = \left(g^{\mu\nu}-\frac{p^\mu p^\nu}{p^2}\right) \times A_{VV'}\left(p^2\right) + \frac{p^\mu p^\nu}{p^2}B_{VV'}\left(p^2\right).$$

The observables are defined as the net contributions from NP:

$$\Delta S = S_{\mathrm{BSM}} - S_{\mathrm{SM}},$$
$$\Delta T = T_{\mathrm{BSM}} - T_{\mathrm{SM}},$$
$$\Delta U = U_{\mathrm{BSM}} - U_{\mathrm{SM}}.$$

The experimental bounds are:

$$\Delta S_{\mathrm{exp}} = 0.021 \pm 0.096,$$
$$\Delta T_{\mathrm{exp}} = 0.040 \pm 0.120,$$
$$\Delta U_{\mathrm{exp}} = 0.008 \pm 0.092.$$

The one-loop vertex correction topologies to the $Z \to \bar{\ell}_\alpha \ell_\beta$ in this BSM model are seen in Figure 4.

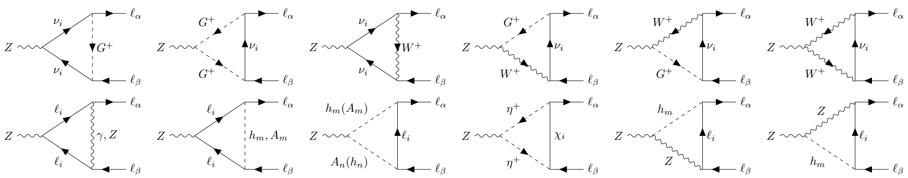

Figure 4: One-loop Feynman diagrams for the $Z \to \bar{\ell}_\alpha \ell_\beta$ vertex corrections within this BSM model.

The one-loop amplitude for $Z \to \bar{\ell}_\alpha \ell_\beta$ can be decomposed in terms of form factors:

$$
\begin{aligned}
&\mathcal{A}\left(Z \to \bar{\ell}_\alpha \ell_\beta\right) \\
&= F_{SL} \psi\left(q_1, m_{\ell_\alpha}\right)\left(\gamma \cdot \epsilon(p)\right) P_L \psi\left(-q_2, m_{\ell_\beta}\right) \\
&+ F_{SR} \psi\left(q_1, m_{\ell_\alpha}\right)\left(\gamma \cdot \epsilon(p)\right) P_R \psi\left(-q_2, m_{\ell_\beta}\right) \\
&+ F_L \psi\left(q_1, m_{\ell_\alpha}\right)\left(q_1 \cdot \epsilon(p)\right) P_L \psi\left(-q_2, m_{\ell_\beta}\right) \\
&+ F_R \psi\left(q_1, m_{\ell_\alpha}\right)\left(q_1 \cdot \epsilon(p)\right) P_R \psi\left(-q_2, m_{\ell_\beta}\right),
\end{aligned}
$$

Considerations for the flavor calculations:

- Feynman t'Hooft gauge $\xi = 1$
- On-shell (OS) renormalization scheme
- $\mathcal{A}_{\mathrm{NP}} = \mathcal{A}_{\mathrm{BSM}} - \mathcal{A}_{\mathrm{SM}}$
- $\mathcal{A}_{\mathrm{finite}} = \mathcal{A}_{\mathrm{VC}} + \mathcal{A}_{\mathrm{CT}}$

Observable	Experimental measurements	SM prediction
$\Gamma\left(Z \to e^+e^-\right)$	$83.91 \pm 0.12\,\mathrm{MeV}$ (LEP [4])	$83.965 \pm 0.016\,\mathrm{MeV}$ [5]
$\Gamma\left(Z \to \mu^+\mu^-\right)$	$83.99 \pm 0.18\,\mathrm{MeV}$ (LEP [4])	$83.965 \pm 0.016\,\mathrm{MeV}$ [5]
$\Gamma\left(Z \to \tau^+\tau^-\right)$	$84.08 \pm 0.22\,\mathrm{MeV}$ (LEP [4])	$83.775 \pm 0.016\,\mathrm{MeV}$ [5]
$\mathrm{BR}\left(Z \to e^\pm\mu^\mp\right)$	$< 4.2 \times 10^{-7}$ (ATLAS [6])	$\mathcal{O}\left(10^{-10}\right)$ (FCC-ee [7])
$\mathrm{BR}\left(Z \to e^\pm\tau^\mp\right)$	$< 4.1 \times 10^{-6}$ (ATLAS [8])	$\mathcal{O}\left(10^{-10}\right)$ (FCC-ee [7])
$\mathrm{BR}\left(Z \to \mu^\pm\tau^\mp\right)$	$< 5.3 \times 10^{-6}$ (ATLAS [8])	$\mathcal{O}\left(10^{-10}\right)$ (FCC-ee [7])
$R_{\mu e}\left(Z \to \ell\ell\right)$	1.0001 ± 0.0024 (PDG [9])	1.0 [5]
$R_{\tau e}\left(Z \to \ell\ell\right)$	1.0020 ± 0.0032 (PDG [9])	0.9977 [5]
$R_{\tau\mu}\left(Z \to \ell\ell\right)$	1.0010 ± 0.0026 (PDG [9])	0.9977 [5]
$\Gamma\left(Z \to \mathrm{Invisible}\right)$	$499.0 \pm 1.5\,\mathrm{MeV}$ (PDG [9])	$501.45 \pm 0.05\,\mathrm{MeV}$ [5]
$\mathrm{BR}\left(H \to \mu^+\mu^-\right)$	$(2.6 \pm 1.3) \times 10^{-4}$ (PDG [9])	$(2.17 \pm 0.13) \times 10^{-4}$ [10]
$\mathrm{BR}\left(H \to \tau^+\tau^-\right)$	$\left(0.06^{+0.008}_{-0.007}\right)$ (PDG [9])	0.0624 ± 0.0035 [10]
$R_{\tau\mu}\left(H \to \ell\ell\right)$	230 ± 146 (PDG [9])	288 [11]

Table 4: Comparison between SM predictions and experimental measurements for flavor-conserving (at 68% C.L.) and flavor-violating leptonic Z/H decays. The lepton flavor universality ratio is defined as $R_{\alpha\beta} \equiv \mathrm{BR}(V \to \ell_\alpha^+\ell_\alpha^-)/\,\mathrm{BR}(V \to \ell_\beta^+\ell_\beta^-)$, where $V = Z, H$. Since the theoretical uncertainties for the SM lepton universality ratios are neligible, only the central values are shown.

4. Flavor and electroweak observables

4.4 EW precision observable: $Z \to \mathrm{Invisible}$

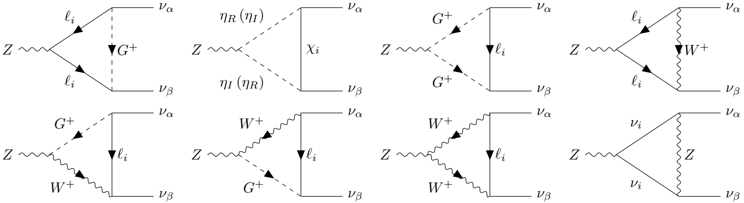

Figure 5: One-loop Feynman diagrams contributing to the $Z \to \mathrm{Invisible}$ decay in this BSM model.

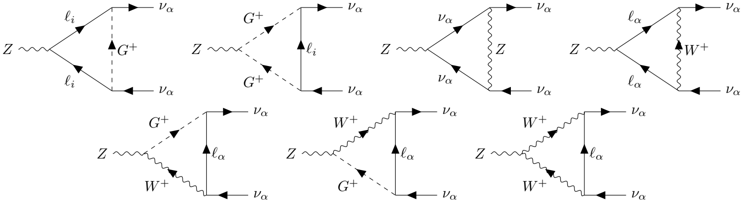

Figure 6: One-loop Feynman diagrams contributing to the $Z \to \mathrm{Invisible}$ decay in the SM.

$$\Gamma_{\mathrm{NP}} \equiv \Gamma_{\mathrm{BSM}} - \Gamma_{\mathrm{SM}} = \sum_{i=1}^{3}\sum_{j=1}^{3} \frac{1}{1+\delta_{ij}} \Gamma\left(Z \to \nu_i \nu_j\right) - \sum_{i=1}^{3} \Gamma\left(Z \to \nu_{i,L} \overline{\nu}_{i,L}\right), \tag{10}$$

4. Flavor and electroweak observables

4.5 EW precision observable: $H \to \bar{\ell}_\alpha \ell_\beta$

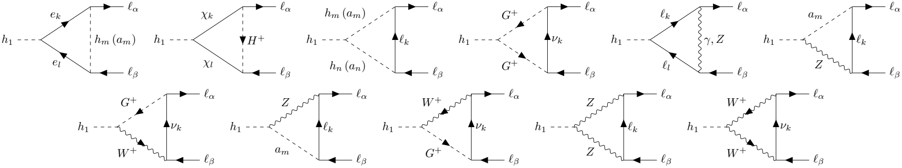

Figure 7: One-loop Feynman diagrams for the $h_1 \to \bar{\ell}_\alpha \ell_\beta$ vertex corrections within this BSM model.

The one-loop amplitude for $H \to \bar{\ell}_\alpha \ell_\beta$ can be decomposed in terms of form factors:

$$\begin{aligned}
&\mathcal{A}\left(H \to \bar{\ell}_\alpha \ell_\beta\right) \\
&= G_L \psi\left(q_1, m_{\ell_\alpha}\right) P_L \psi\left(-q_2, m_{\ell_\beta}\right) \\
&+ G_R \psi\left(q_1, m_{\ell_\alpha}\right) P_R \psi\left(-q_2, m_{\ell_\beta}\right).
\end{aligned}$$

$$\begin{aligned}
&2\,\mathrm{Re}\left[\mathcal{A}_{\text{tree}}\left(h_1 \to \ell\ell\right)\left(\mathcal{A}_{\text{OL}}\left(h_1 \to \ell\ell\right)\right)^*\right] \\
&+ \left|\mathcal{A}_{\text{soft}}\left(h_1 \to \ell\ell\gamma\right)\right|^2 = 0
\end{aligned}$$

$$\begin{aligned}
&\left|\mathcal{A}_{\text{soft}}\left(h_1 \to \ell\ell\gamma\right)\right|^2 \approx \left|\mathcal{A}_{\text{Born}}\left(h_1 \to \ell\ell\right)\right|^2 \\
&\times \left(\frac{c_{20}}{\left(q_1 \cdot k\right)^2} + \frac{c_{11}}{\left(q_1 \cdot k\right)\left(q_2 \cdot k\right)} + \frac{c_{02}}{\left(q_2 \cdot k\right)^2}\right).
\end{aligned}$$

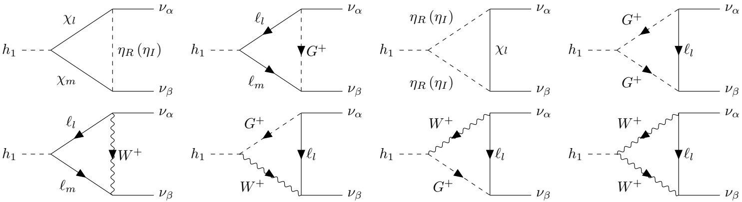

Figure 8: One-loop Feynman diagrams contributing to the $h_1 \to \mathrm{Invisible}$ vertex corrections within this BSM model.

Since there is no tree-level $H\nu\nu$ interaction, no counter-terms are required. The $H \to \mathrm{Invisible}$ is a purely NP effect.

Table of Contents

5. Numerical analysis

5.1 Neutrino mass hierarchies

The scanned neutrino mass spectra in both hierarchies are as follows:

	Normal hierarchy		Inverted hierarchy	
	Minimum value	Maximum value	Minimum value	Maximum value
m_{ν_1}	1.0008×10^{-19}	2.1409×10^{-11}	4.9376×10^{-11}	4.9649×10^{-11}
m_{ν_2}	8.3196×10^{-12}	2.3129×10^{-11}	5.0076×10^{-11}	5.0399×10^{-11}
m_{ν_3}	5.0332×10^{-11}	5.5482×10^{-11}	1.0005×10^{-19}	5.1159×10^{-13}
$\sum_{i=1}^{3} m_{\nu_i}$	5.8698×10^{-11}	9.9913×10^{-11}	9.9453×10^{-11}	1.0000×10^{-10}

Table 5: Minimum and maximum values of the neutrino masses obtained from the parameter scan, for both normal hierarchy and inverted hierarchy. All retained points satisfy the neutrino mass-squared difference constraints at the 3σ level.

The experimental bounds considered in this work are the following:

- The cosmological upper bound on the sum of neutrino masses [12], $\sum_{i=1}^{3} m_{\nu_i} \leq 10^{-10}\,\mathrm{GeV}$
- The DESI BAO measurement to $\sum_{i=1}^{3} m_{\nu_i} < 6.42 \times 10^{-11}\,\mathrm{GeV}$ [13] - Inverted hierarchy is likely to be ruled out

5. Numerical analysis

5.2 DM analysis

In this BSM model, there are three DM candidates: $\eta_{R,I}$ and χ_1, but only two of them - χ_1 and η_I - remain viable given the resulting mass spectrum.

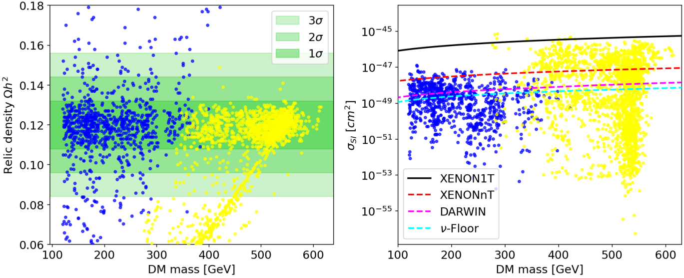

Figure 9: Scanned DM mass versus relic density (left panel) and spin-independent proton cross section (right panel). In both panels, blue points correspond to the fermionic DM candidate χ_1, while yellow points correspond to the CP-odd scalar DM candidate η_I. In the right panel, the current experimental upper bound from XENON1T [14] and future sensitivities from XENONnT [15], DARWIN [16], and the neutrino floor (ν-floor) [17] are also shown.

- The fermionic DM candidate χ_1 accounts for 29%, while the scalar DM η_I accounts for 71%.
- χ_1 ranges from 120 to $350\,\mathrm{GeV}$, while η_I ranges from 350 to $600\,\mathrm{GeV}$.
- A large number of points survive the constraints from the DM experiments.

5. Numerical analysis

5.3 Flavor observable analysis

$$
\begin{aligned}
\mathcal{O}\left(\Delta a_\mu\right) &= 10^{-14}, \\
\mathcal{O}\left(\mathcal{B}\left(\mu \to e\gamma\right)\right) &= [10^{-35}, 10^{-26}], \\
\mathcal{O}\left(\mathcal{B}\left(\tau \to e\gamma\right)\right) &= [10^{-35}, 10^{-26}], \\
\mathcal{O}\left(\mathcal{B}\left(\tau \to \mu\gamma\right)\right) &= [10^{-33}, 10^{-25}], \\
\mathcal{O}\left(\mathcal{B}\left(\mu \to e, \mathrm{Al}\right)\right) &= [10^{-37}, 10^{-28}], \\
\mathcal{O}\left(\mathcal{B}\left(\mu \to 3e\right)\right) &= [10^{-36}, 10^{-28}], \\
\mathcal{O}\left(\mathcal{B}\left(\tau \to 3e\right)\right) &= [10^{-36}, 10^{-28}], \\
\mathcal{O}\left(\mathcal{B}\left(\tau \to 3\mu\right)\right) &= [10^{-35}, 10^{-27}], \\
\mathcal{O}\left(\mathcal{B}\left(Z \to e^\pm \mu^\mp\right)\right) &= [10^{-40}, 10^{-31}], \\
\mathcal{O}\left(\mathcal{B}\left(Z \to e^\pm \tau^\mp\right)\right) &= [10^{-38}, 10^{-30}], \\
\mathcal{O}\left(\mathcal{B}\left(Z \to \mu^\pm \tau^\mp\right)\right) &= [10^{-37}, 10^{-29}], \\
\mathcal{O}\left(\mathcal{B}\left(H \to e^\pm \mu^\mp\right)\right) &= [10^{-46}, 10^{-33}], \\
\mathcal{O}\left(\mathcal{B}\left(H \to e^\pm \tau^\mp\right)\right) &= [10^{-43}, 10^{-30}], \\
\mathcal{O}\left(\mathcal{B}\left(H \to \mu^\pm \tau^\mp\right)\right) &= [10^{-44}, 10^{-29}].
\end{aligned}
$$

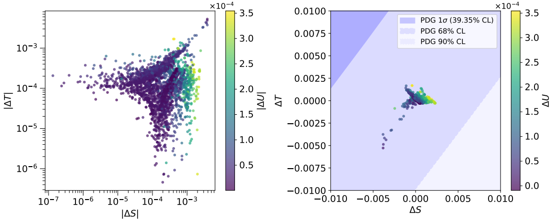

Figure 10: Scanned results of the oblique parameters

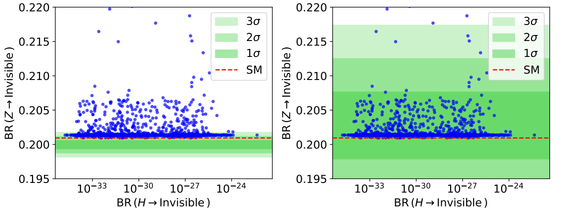

Figure 11: Scanned results of $H \to \mathrm{Invisible}$ versus $Z \to \mathrm{Invisible}$. The left panel is based on the world average experimental bound, whereas the right panel is based on the recent ATLAS experimental bound [18]

.

Table of Contents

6. Conclusion

We perform a global analysis of a minimally extended scotogenic model motivated by observed non-zero neutrino masses, viable dark matter (DM) candidates, and the instability of the Standard Model (SM) vacuum at high-energies.

We examine the bounded-from-below conditions, vacuum stability, and RG-driven perturbativity bounds arising from the extended scalar sector, alongside a comprehensive set of flavor and electroweak (EW) precision observables.

Under these considerations, the main findings are as follows:

1. the DESI BAO bound would rule out the inverted hierarchy if confirmed by other experiments.
2. the oblique parameters are projected to be within the reach of future precision measurements.
3. the viable fermionic DM candidate mass lies in the range $120 - 350\,\mathrm{GeV}$, while the CP-odd scalar is constrained to $350 - 600\,\mathrm{GeV}$.
4. our result on $Z \to \mathrm{Invisible}$ is compatible with the world average at the 3σ level and is favored by the recent ATLAS measurement at the 3σ level.

References I

Ivan Esteban, M. C. Gonzalez-Garcia, Michele Maltoni, Ivan Martinez-Soler, João Paulo Pinheiro, and Thomas Schwetz.

NuFit-6.0: updated global analysis of three-flavor neutrino oscillations.

JHEP, 12:216, 2024.

Dario Buttazzo, Giuseppe Degrassi, Pier Paolo Giardino, Gian F. Giudice, Filippo Sala, Alberto Salvio, and Alessandro Strumia.

Investigating the near-criticality of the Higgs boson.

JHEP, 12:089, 2013.

Gudrun Hiller, Tim Höhne, Daniel F. Litim, and Tom Steudtner.

Vacuum stability in the Standard Model and beyond.

Phys. Rev. D, 110(11):115017, 2024.

S. Schael et al.

Precision electroweak measurements on the Z resonance.

Phys. Rept., 427:257–454, 2006.

References II

Ayres Freitas.

Higher-order electroweak corrections to the partial widths and branching ratios of the Z boson.

JHEP, 04:070, 2014.

Georges Aad et al.

Search for the lepton flavor violating decay Z→eμ in pp collisions at $\sqrt{s}$ TeV with the ATLAS detector.

Phys. Rev. D, 90(7):072010, 2014.

A. Abada et al.

FCC Physics Opportunities: Future Circular Collider Conceptual Design Report Volume 1.

Eur. Phys. J. C, 79(6):474, 2019.

Georges Aad et al.

Search for lepton-flavor-violation in Z-boson decays with τ-leptons with the ATLAS detector.

Phys. Rev. Lett., 127:271801, 2022.

References III

S. Navas et al.

Review of particle physics.

Phys. Rev. D, 110(3):030001, 2024.

A. Denner, S. Heinemeyer, I. Puljak, D. Rebuzzi, and M. Spira.

Standard Model Higgs-Boson Branching Ratios with Uncertainties.

Eur. Phys. J. C, 71:1753, 2011.

D. de Florian et al.

Handbook of LHC Higgs Cross Sections: 4. Deciphering the Nature of the Higgs Sector.

CERN Yellow Rep. Monogr., 2:1–869, 2017.

N. Aghanim et al.

Planck 2018 results. VI. Cosmological parameters.

Astron. Astrophys., 641:A6, 2020.

[Erratum: Astron.Astrophys. 652, C4 (2021)].

References IV

W. Elbers et al.

Constraints on neutrino physics from DESI DR2 BAO and DR1 full shape.

Phys. Rev. D, 112(8):083513, 2025.

E. Aprile et al.

Dark Matter Search Results from a One Ton-Year Exposure of XENON1T.

Phys. Rev. Lett., 121(11):111302, 2018.

E. Aprile et al.

Projected WIMP sensitivity of the XENONnT dark matter experiment.

JCAP, 11:031, 2020.

J. Aalbers et al.

DARWIN: towards the ultimate dark matter detector.

JCAP, 11:017, 2016.

References V

Ciaran A. J. O'Hare.

New Definition of the Neutrino Floor for Direct Dark Matter Searches.

Phys. Rev. Lett., 127(25):251802, 2021.

Georges Aad et al.

Measurement of the Z boson invisible width at s=13 TeV with the ATLAS detector.

Phys. Lett. B, 854:138705, 2024.